Migration of Constant Offset Sections

Rick Ottolini

A phase shift prestack migration algorithm (Hale, previous paper) is used to migrate constant offset sections. It images the steep dips and wide offsets of a constant velocity synthetic quite well. It works worse on a variable velocity synthetic and real data.

Computer Algorithm

The algorithm which images constant offset sections has two steps. First, the constant offset section is converted into a zero offset section. The phase shift equation which does this is derived by Hale elsewhere in this SEP volume. In brief, a substitution is made in the double square equation which makes it convert constant offset sections into unmigrated zero offset sections instead of into migrated zero offset sections. The result is the single square root equation:

$$P(\omega_0,k_x) = \sum_{t_h} P(t_h,k_x) \exp\left(i\omega_0 \left[t_h^2 - \frac{4h^2}{v^2}\left[1 - \frac{v^2 k_x^2}{4\omega_0^2} \right] \right]^{1/2} \right) \qquad (1)$$

where t_h is the two way travel time at half-offset h. t_0 and ω_0 correspond to unmigrated zero offset two way travel time. (An amplitude correction term has been dropped from Hale's derivation.) For zero offset, h=0, equation 1 reduces to a Fourier transform.

The second imaging step is to migrate the resulting zero offset section using conventional migration. The phase shift equation which does this is

$$P(t_m,k_x) = \sum_{\omega_0} P(\omega_0,k_x) \exp\left[-it_m \left(4\omega_0^2 - v^2 k_x^2 \right)^{1/2} \right] \qquad (2)$$

where t_m is migrated zero offset two-way travel time.

A computer program may be written to migrate constant offset sections. The program is almost as efficient as migrating a zero offset section. It is outlined as follows:

```
Fourier transform P(t,x) → P(t,k_x)
for each k_x
    for each causal t_h
        for each ω_0
            multiply P(t_h,k_x) times exponential (1)
            sum into result P(ω_0,k_x)
x   inverse Fourier transform P(ω_0,k_x) → P(t_0,k_x)
x   inverse Fourier transform P(t_0,k_x) → P(t_0,x)
x   Fourier transform P(t_0,x) → P(t_0,k_x)
x   for each k_x
    Fourier transform P(t_0,k_x) → P(ω_0,k_x)
    for each ω_0
        for each t_m
            multiply P(ω_0,k_x) times exponential (2)
            sum into result P(t_m,k_x)
inverse Fourier transform P(t_m,k_x) → P(t_m,x)
```

The portion which does equation 1 resembles a modeling algorithm in an operational sense, while the portion which does equation 2 resembles a migration algorithm. By joining both operations, the four middle Fourier transforms can be eliminated (lines marked with an x). The k_x loop can be done all in one subroutine call using a custom array processor vector routine.

Constant Velocity Example

Figure 1 is the constant velocity earth model. There are five straight reflectors tilting between 0 and 80 degrees from the horizontal. Analytical ray tracing (Slotnick, 1959) was used to generate 200 common midpoint gathers. Figure 2 contains selected unmigrated common offset sections. It demonstrates offset dependent moveout and lateral shifts. Figure 3 shows these constant offset sections migrated. Migration has corrected for moveout and lateral shifts. Figure 4 shows selected common midpoint gathers. Notice that events with different dips have different moveout functions. This causes a multi-value stacking velocity problem when stacking intersecting reflections. Figure 5 displays the same gathers from migrated constant offset sections. Migration has corrected for moveout, correctly alleviating dip effects. It works well for wide offsets and steep dips. Figure 6 contains a stack of the migrated constant offset section compared to a migration of the zero offset section and conventional stack. This constant offset section migration algorithm works as

well or better than other migration algorithms on constant velocity synthetics.

Depth Variable Velocity

Two methods of incorporating depth variable velocities were tried.

(1) Consider the media be a pile of thin constant velocity layers. The wavefield is continued by a constant velocity algorithm through each layer. The cumulative phase shift at depth z is given by the integral

$$\int_0^z dz \frac{\partial \Phi(z)}{\partial z} \tag{3}$$

where Φ is the constant velocity phase shift.

This integral is easy to compute when Φ is a simple function of depth, as in the case of migrating zero offset sections. However, this is not the case for equation 1. I abandoned this approach after several unsuccessful attempts.

(2) Another method is to replace interval velocity in equation 1 with rms velocity. This is analogous to conventional normal moveout. As with conventional normal moveout, this approximation deteriorates with increasing dip and offset and sharp velocity variations.

Equation 1 can be applied to constant offset sections which have been corrected for normal moveout. Then the part of equation which does normal moveout correction, $\frac{4h^2}{v^2}$, should be removed. Both approaches give about the same result.

Variable Velocity Example

Figure 7 is the variable velocity earth model. Straight layers tilt from 0 to 80 degrees. Velocity increases linearly with depth. Ray tracing (Slotnick, 1959) was used to generate 200 common midpoint gathers. Figure 8 contains selected constant offset sections. Figure 9 shows the same constant offset section normal moved out. Dipping events at different offsets do not laterally align. Figure 10 displays migrated constant sections. These were migrated using rms velocities. The lateral alignment of dipping beds is much better, although not perfect. Figure 11 shows selected common midpoint gathers. Figure 12 has the same common midpoint gathers from migrated constant offset sections. Migration quality deteriorates at increasingly steep dips and wide offsets. Figure 13 compares the stack of the migrated constant offset sections with migrations of the zero offset section and conventional stack. This depth variable velocity algorithm is not the worst result, though it is

not the best.

Field Data Example

Constant offset sections of a field data growth fault were migrated. Experiments using stacking velocities that are too high suggest that migration before stack should image more of the fault plane reflection than conventional processing. Figure 14 compares the migration of constant offset sections to migration after conventional stacking. There is little significant difference between the two. Figure 15 shows a common midpoint gather taken from constant offset sections before and after migration. It demonstrates that migration corrects for offset dependent moveout.

Conclusions

This constant offset section migration algorithm performs rather well on constant velocity synthetics. It works better than conventional processing on depth variable velocity synthetics. It shows little improvement over conventional processing of field data.

Appendix: Equations for Generating Synthetics

Travel time equations for separated sources and receivers were adapted from Slotnick. Consider the geometry shown in figure A1. In a constant velocity media travel time is given by

$$t = \frac{1}{v}\sqrt{f^2 + 4s\sin\alpha(s + f)} \tag{A1}$$

This formula can be derived by putting a mirror image of the seismic experiment on the other side of the reflector.

I could derive a fully analytic expression for two-way reflection travel time in a depth variable velocity medium. Instead, analytic expressions for one way travel time were combined and searched for the minimum. Given a linearly increasing velocity function of the form $v_0 + az$, Slotnick showed that the normal incidence raypath to a dipping reflector is a circular arc with a travel time

$$t = \frac{1}{a}\cosh^{-1}\left[1 + \frac{a^2(x^2 + z^2)}{2v_0(v_0 + az)}\right] \tag{A2}$$

The raypath arcs from the source and to the receiver are constrained to meet at the

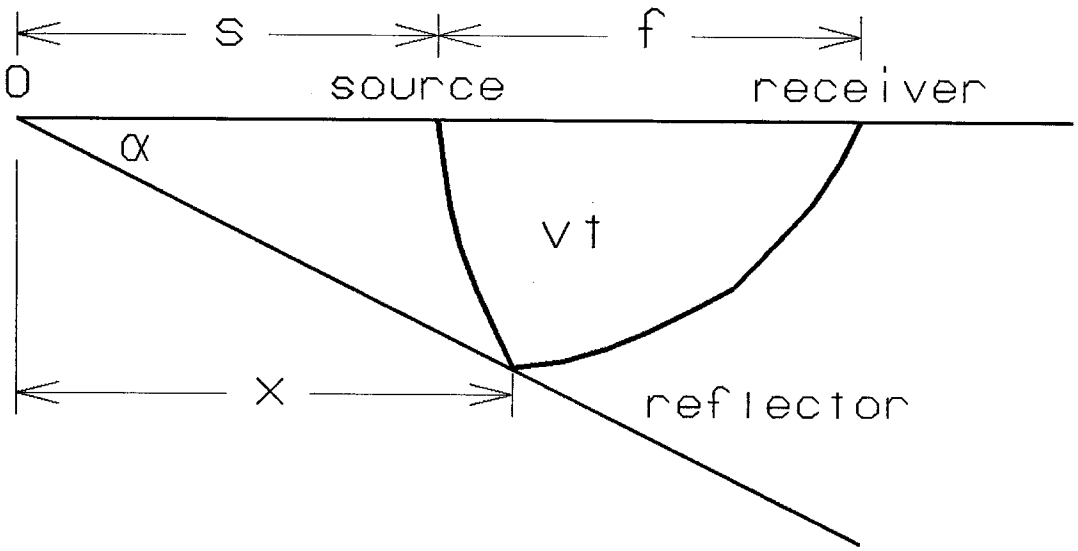

FIG. A1. Geometry for ray tracing in a depth variable velocity media. Minimum travel time raypaths to the reflector are circular arcs. If velocity is constant, then the raypaths are straight lines.

reflector. The combined travel time is

$$t = \left\{ \cosh^{-1}\left[1 + \frac{a^2[(s+f-x)^2 + (x\tan\alpha)^2]}{2v_0(v_0 + ax\tan\alpha)}\right] + \cosh^{-1}\left[1 + \frac{a^2[(x-s)^2 + (x\tan\alpha)^2]}{2v_0(v_0 + ax\tan\alpha)}\right]\right\} \tag{A3}$$

Travel time is minimized with respect to the free parameter x.

REFERENCE

Slotnick, M.M., 1959, Lessons in seismic computing, edited by R.A. Geyer, SEG, Tulsa

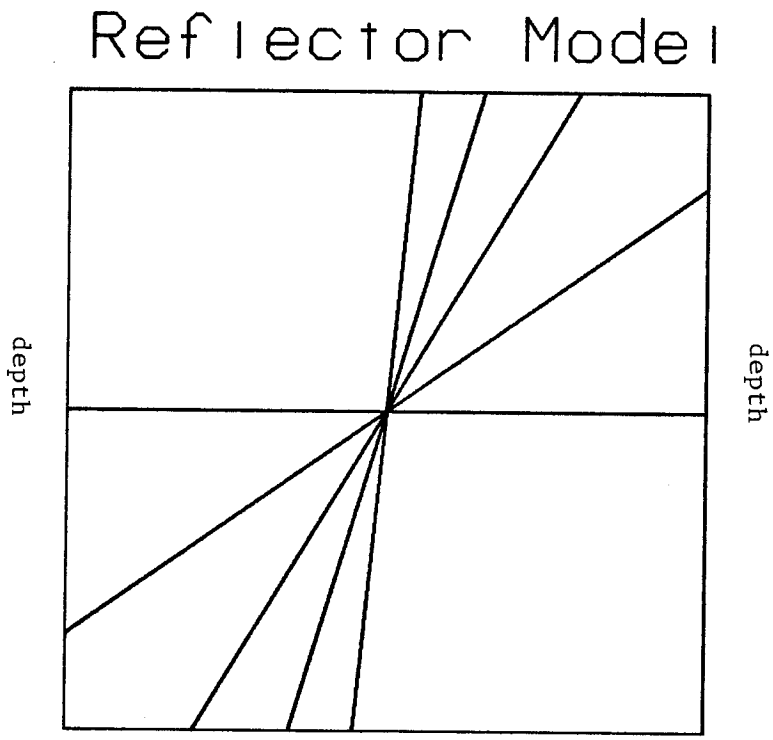

Figure 1. Reflector model for generating constant velocity synthetics. Five straight reflectors dip from 0 to 80 degrees at 20 degree increments. An analytic ray tracing expression was used to generate synthetic seismograms. Parameters are: nx=200, dx=.5, nt=100, dt=1., $noff$=100, $doff$=1., v=1.; A (1,3,1) wavelet was convolved onto the travel times. Amplitude variations were not considered in the model.

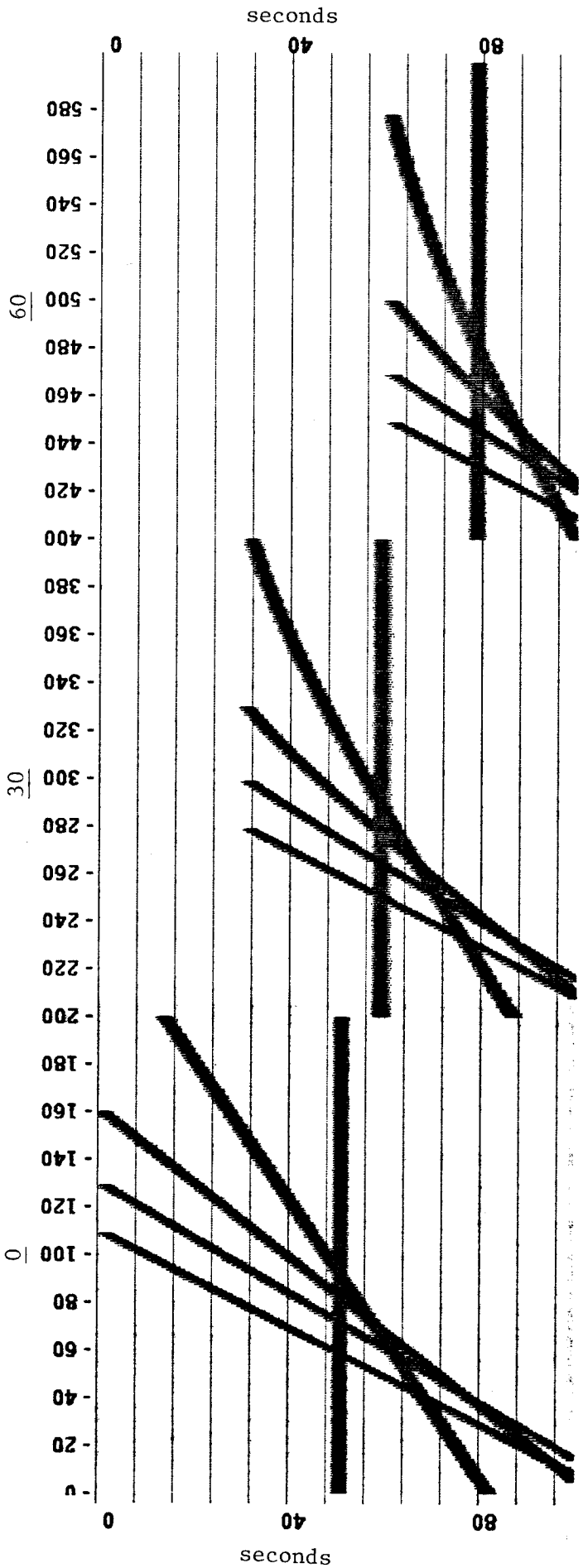

Figure 2. Selected unmigrated common offset sections. Underlined title numbers refer to offset panel. Notice the offset dependent moveout and lateral shifts.

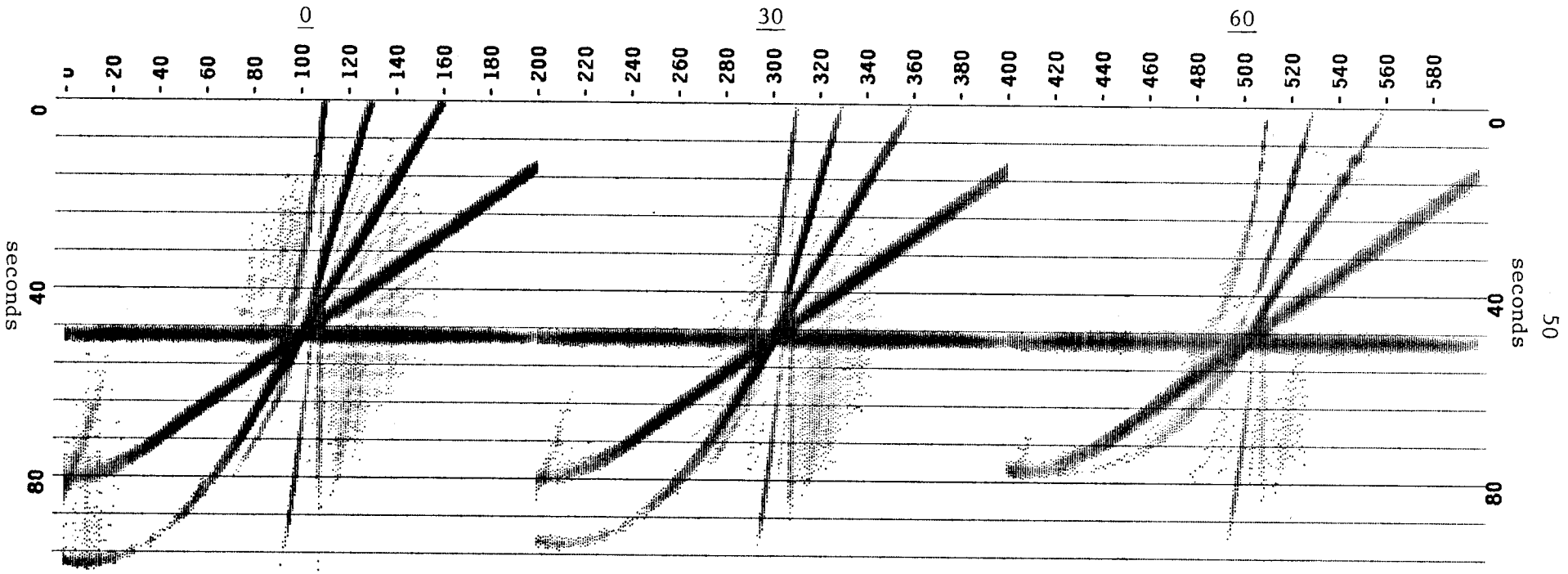

Figure 3. Migrated common offset sections from figure 2. The common offset migration algorithm automatically applies normal moveout. Reflectors of the same dip are laterally aligned after migration.

There are a few artifacts, however. None are serious defects of the constant offset migration algorithm. First is wrap around across the time directions due to the frequency domain migration algorithm. Second are curved tails appended to the lower left of dipping reflectors caused by the sudden truncation of data at the boundaries. Third is the absence of the steeper reflectors at high time values due to not computing long enough travel times for the seismograms. Fourth is some random noise near the middle of each section probably caused by not zeroing evanescent energy during the course of migration entirely correct.

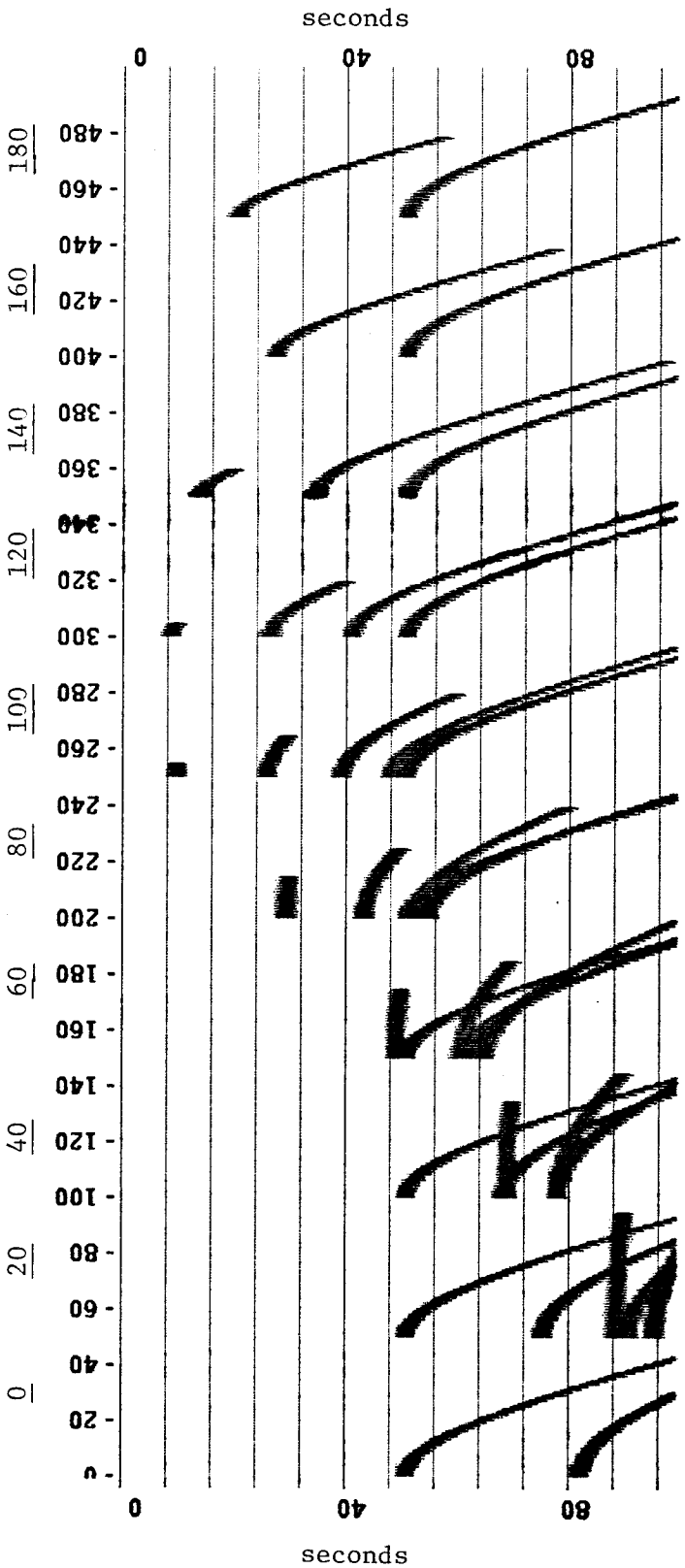

Figure 4. Selected unmigrated common midpoint gathers. The underlined title numbers refer to midpoint locations. Notice that events with different dips have different moveout functions. This causes multi-value stacking velocity problems when stacking intersecting reflectors.

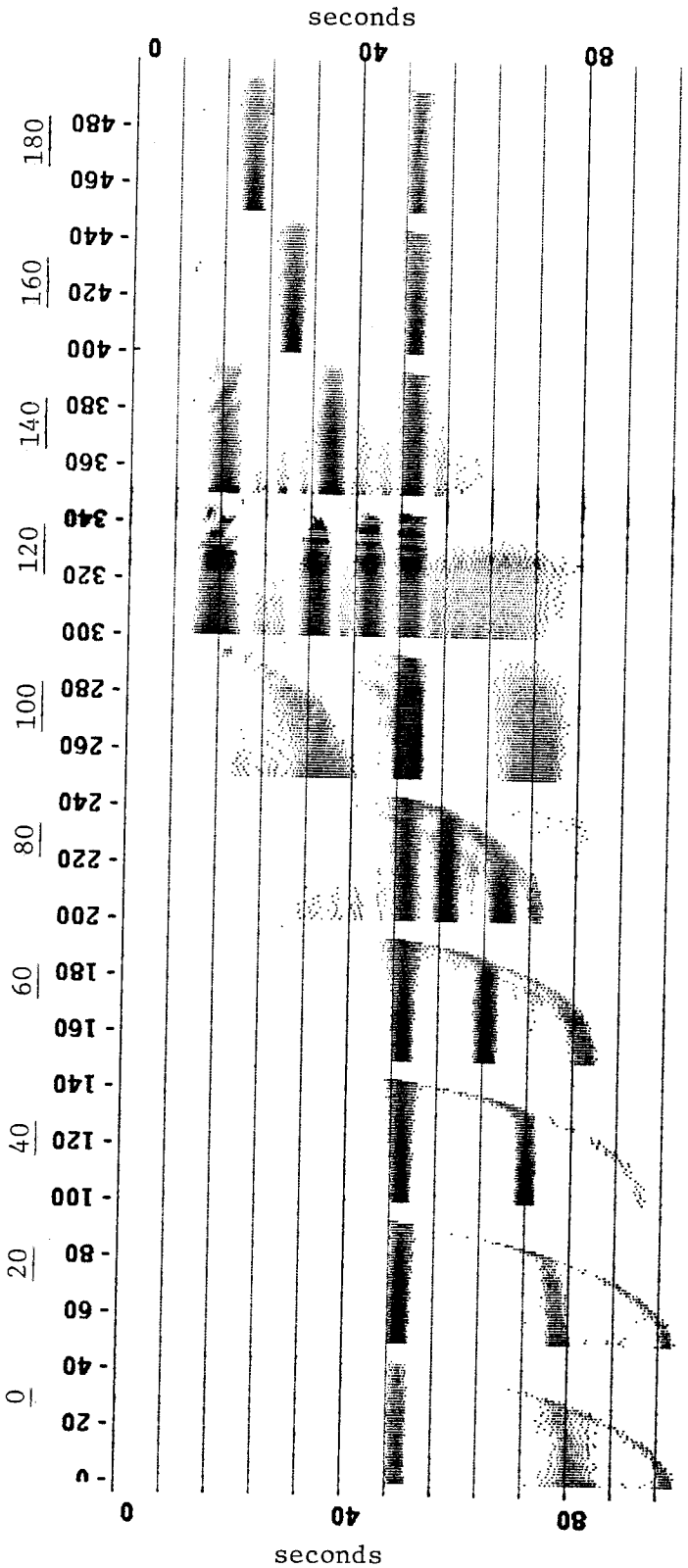

Figure 5. Common midpoint gathers from migrated constant offset sections. They are from the same midpoints as in the previous figure. Reflectors at steep dips and wide offsets are moved out correctly.

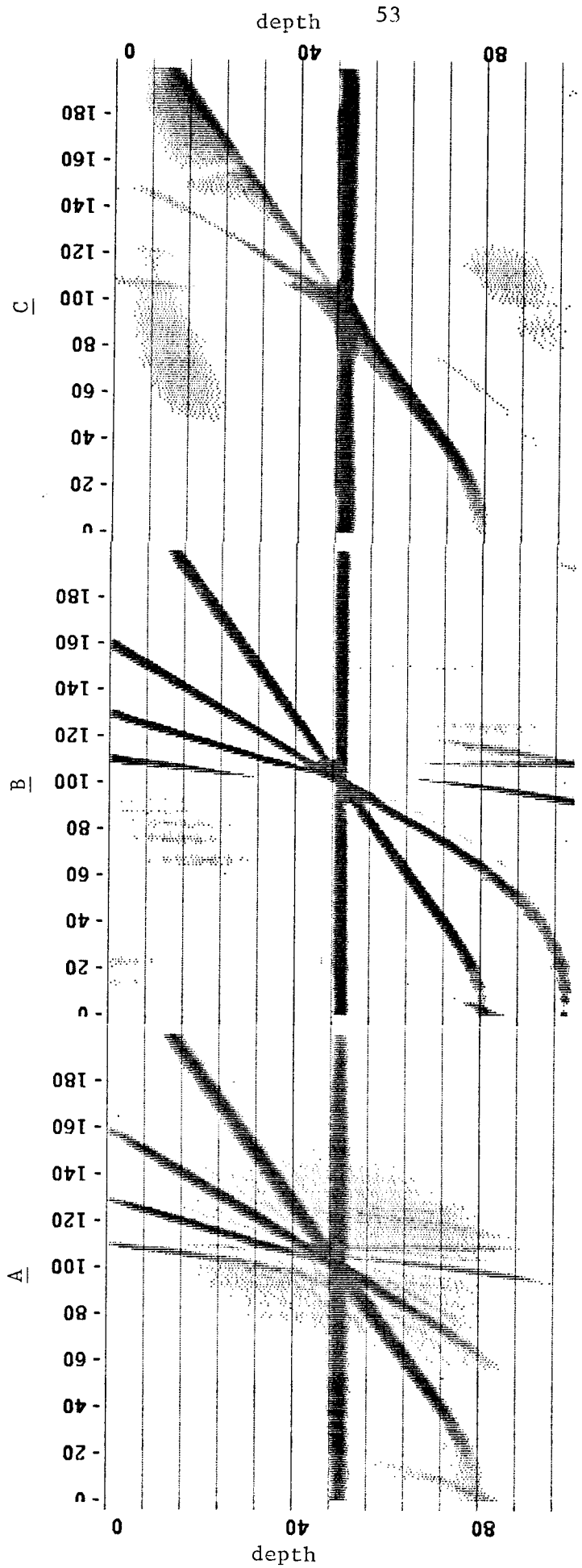

Figure 6. (A) Stack of migrated common offset sections. Fifty sections, at every other offset, were included. All reflector dips are correctly imaged. The results are as good as, or better than, other migration algorithms implemented in the frequency domain. Artifacts are explained in the figure 3 caption. (B) Migrated zero offset section. This is the standard with which to compare other migration results. (C) Migrated conventional stack. Conventional processing does not handle steep dip - wide offset reflections well.

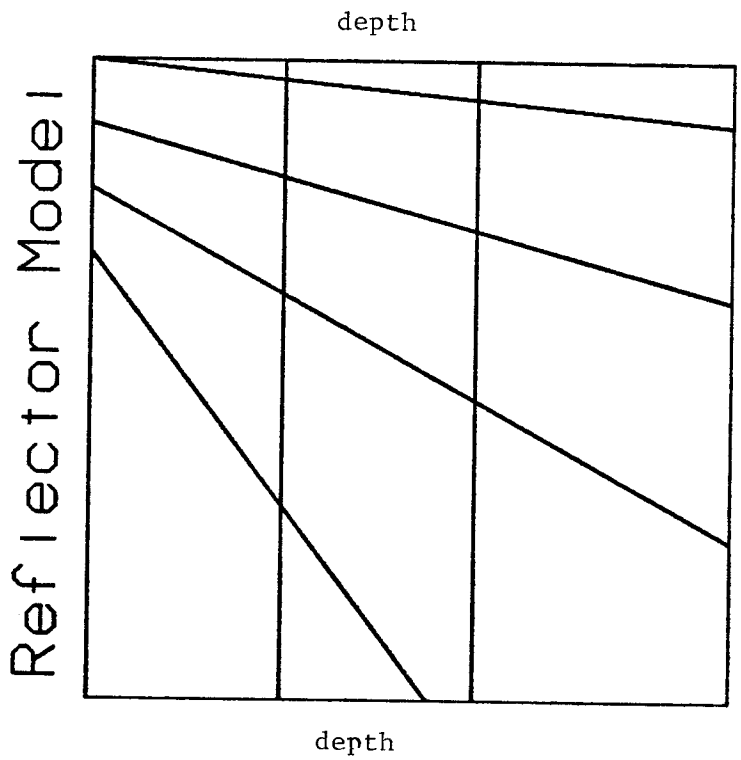

Figure 7. Reflector model for generating depth variable velocity synthetics. Straight reflectors dip from 0 to 80 degrees at 20 degree increments. The velocity increases linearly with depth. Ray tracing (Slotnick, 1959) was used to generate synthetic seismograms. Parameters are: nx=200, dx=.5, nt=256, dt=1., nz=100, dz=1., $v0$=.5, dv/dz=.01, $nofs$=100, $dofs$=.8. A (1,3,1) wavelet was convolved onto the travel times. Amplitude effects were not considered in the model.

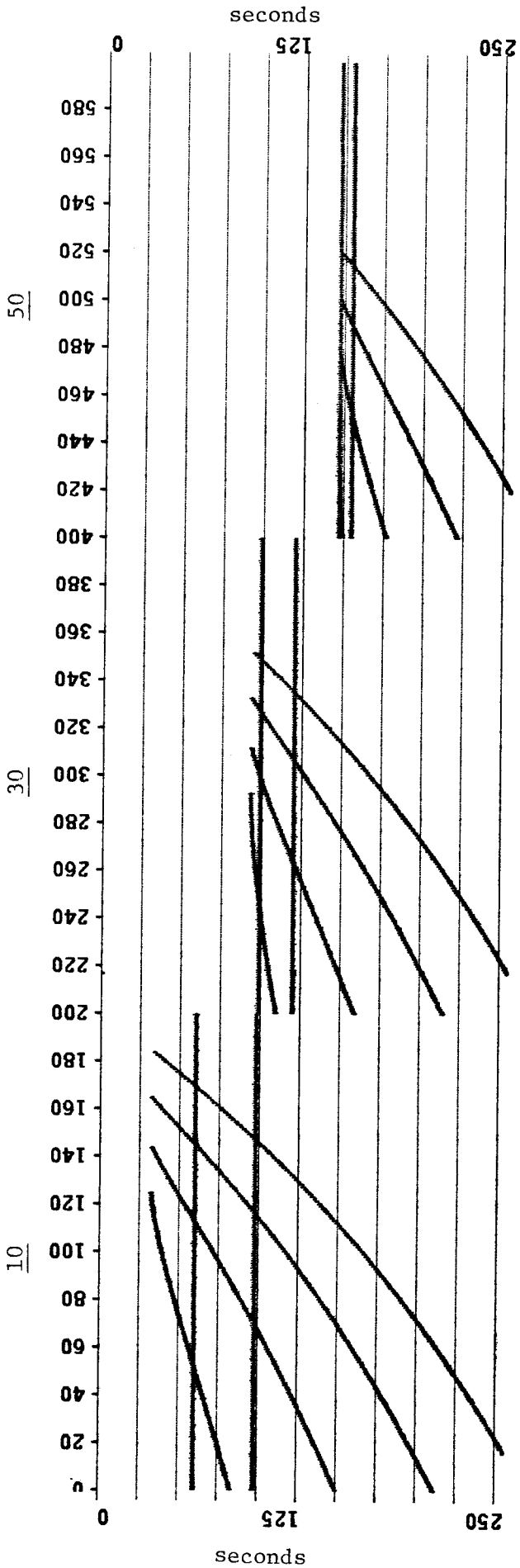

Figure 8. Selected constant offset sections. Underlined title numbers refer to offset. Zero offset is not shown.

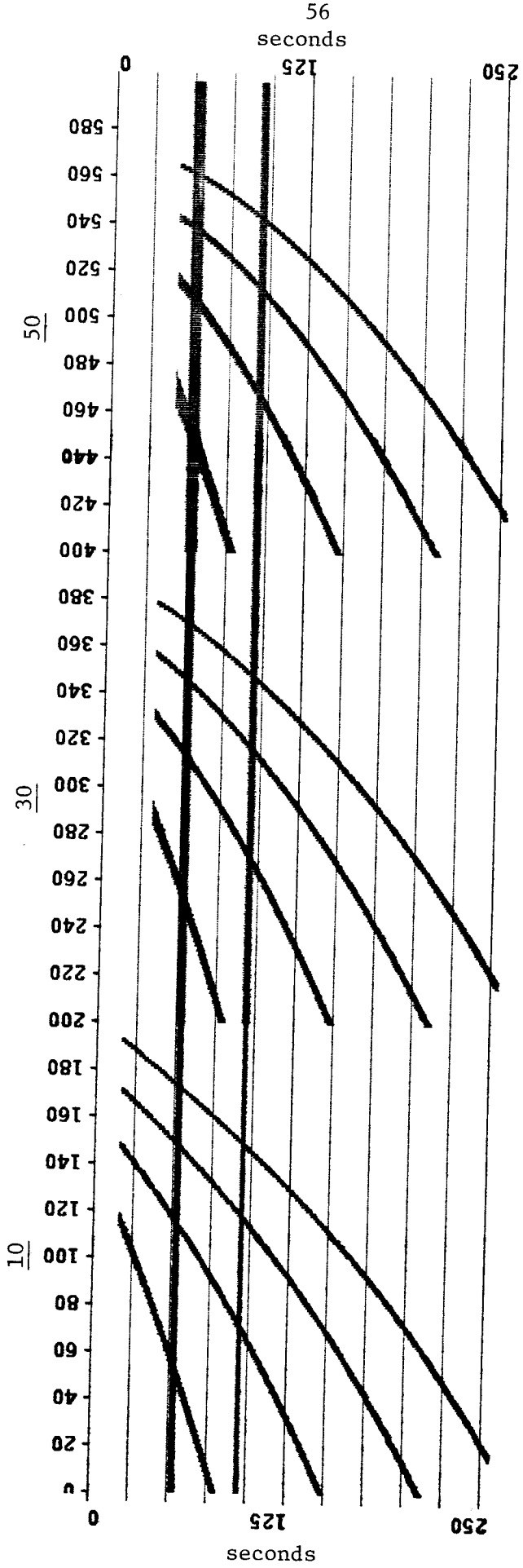

Figure 9. The constant offset sections from figure 8 are now normal moved out. Severe moveout stretch was muted out. Note that steeper dipping reflectors do not laterally align between different offsets.

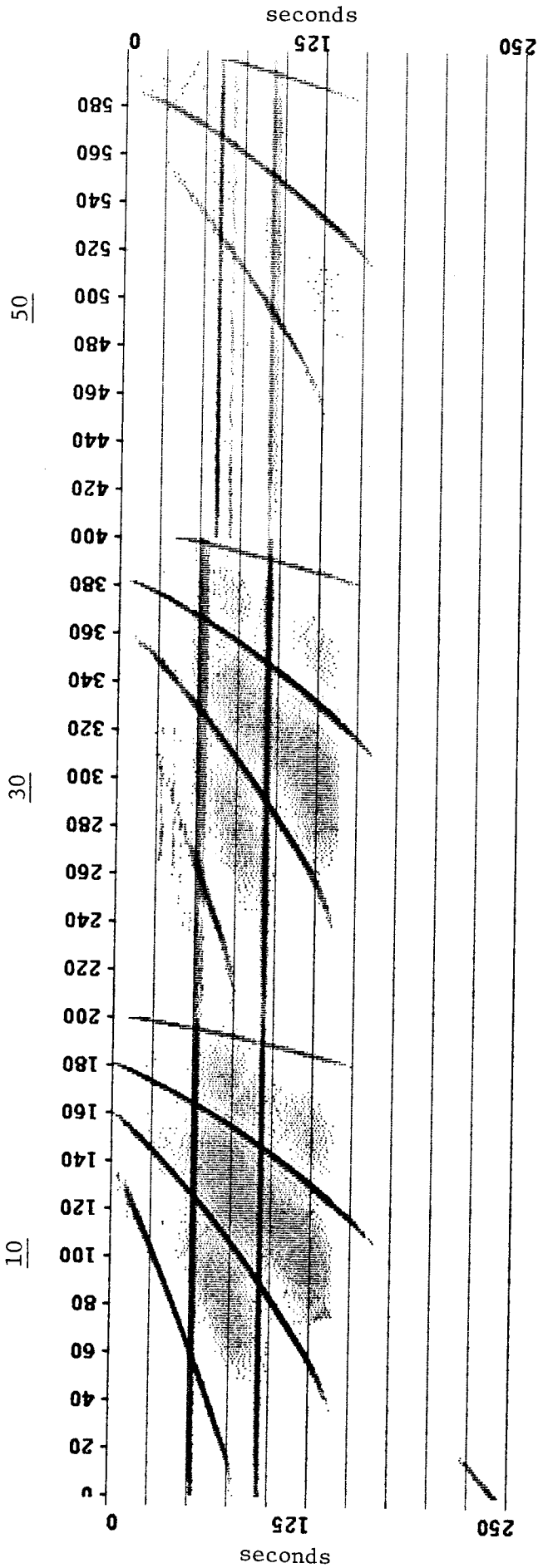

Figure 10. The constant offset sections from figure 8 now migrated. Migration automatically applies normal moveout. The third panel is from a relatively wide offset where the upper reflector is just beyond critical reflection. The lateral alignment of dipping events across different offsets is much improved after migration, though not perfect. Other migration artifacts are the same as in the caption for figure 3.

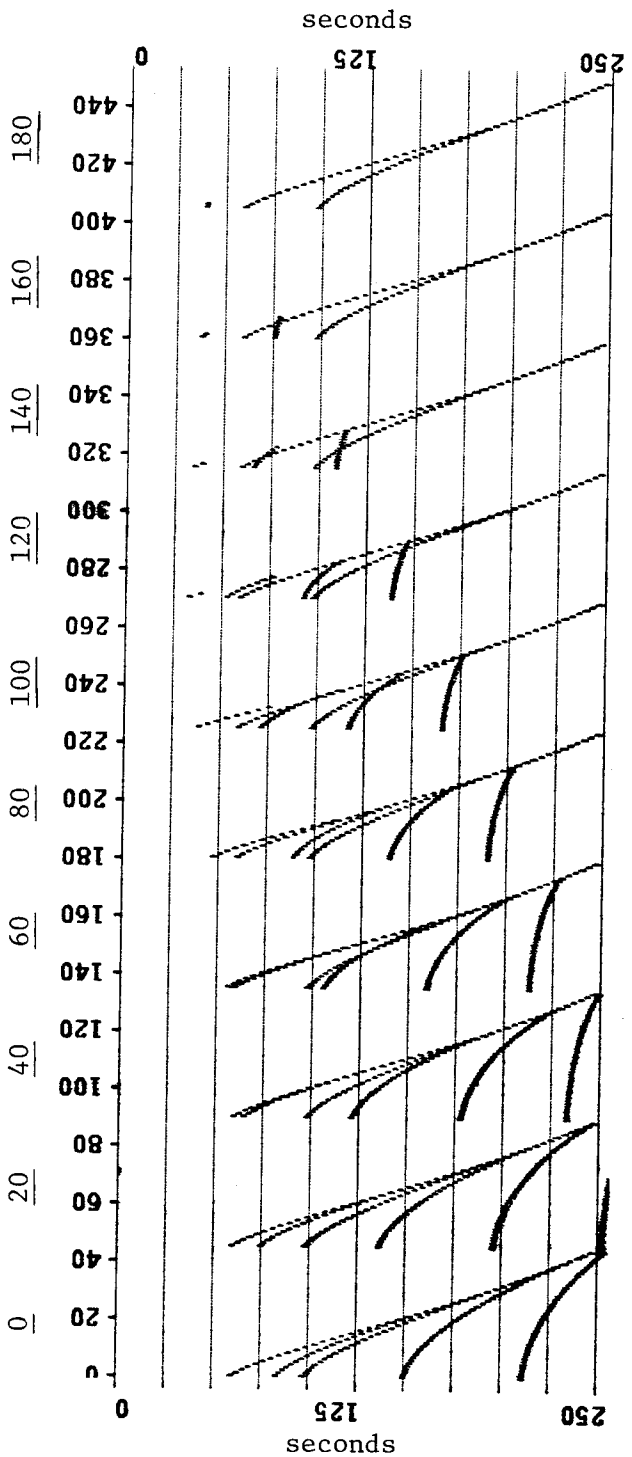

Figure 11. Selected unmigrated common midpoint gathers. The underlined title number refers to midpoint.

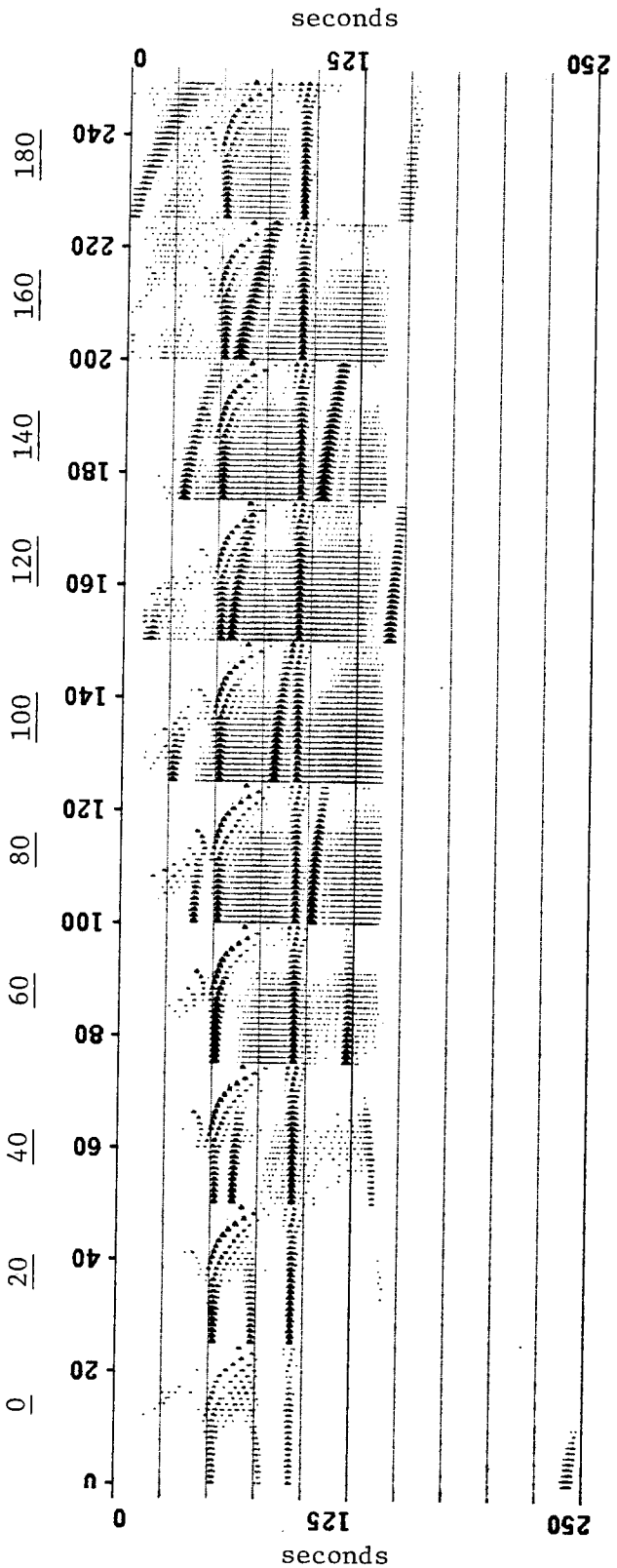

Figure 12. Common midpoint gathers from migrated constant offset sections. They are from the same midpoints as in the previous figure. Flat dip rms velocities were used in the migration algorithm to approximate depth variable velocity. The moveout correction becomes increasingly bad for steeper dips and wider offsets.

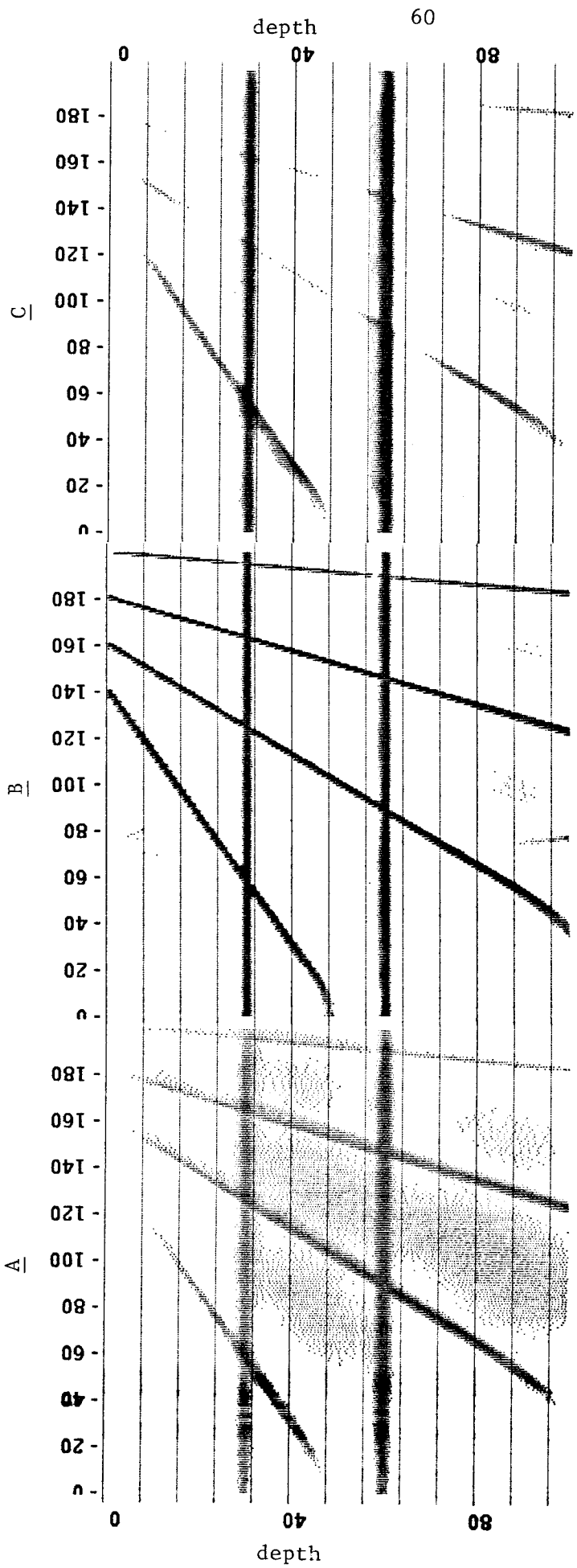

Figure 13. (A) Stack of 20 migrated constant offset sections. The 10 nearest offsets were not included. The result is better than conventional processing, although not as good as those from some other migration methods. Dipping events are degraded slightly. (B) Migrated zero offset section. This is the standard with which to compare other migration results. (C) Migrated conventional stack. Conventional processing does not handle steep dip - wide offset reflections well.

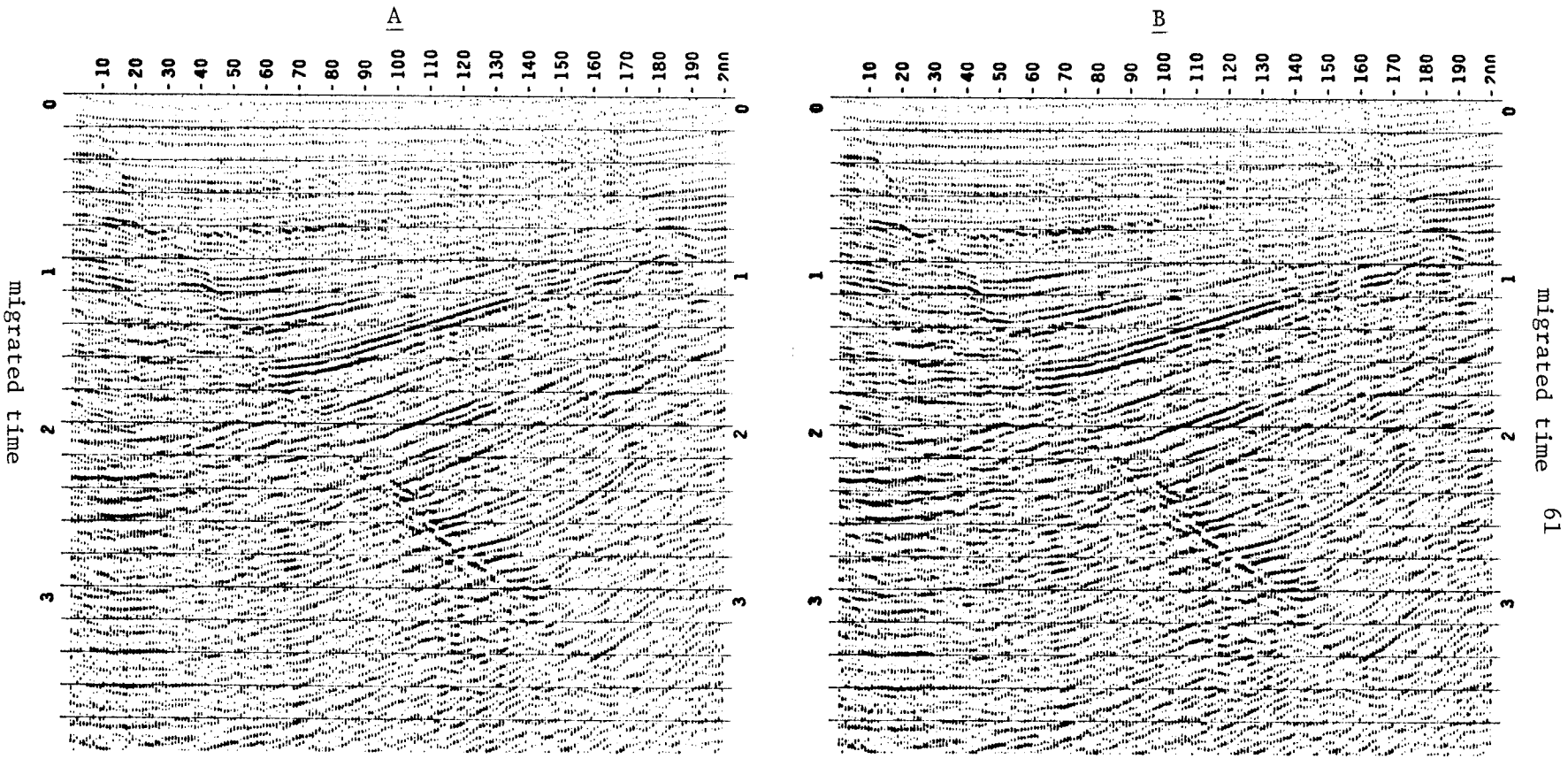

Figure 14. (A) Conventional stacking and migration of field data containing a growth fault. (B) Stack of migrated constant offset sections. The migration before stack result is not appreciably different from conventional processing. For both cases, the original data volume was reduced by a factor of three by summing three adjacent offsets. Some data parameters are nx=200, dx=166', nt=1024, dt=.004, $noff$=16, $near$=1204', $doff \approx$ 500', $vmax$=10,200'/s, $tmin$=1.0s, $tmax$=5.0s.

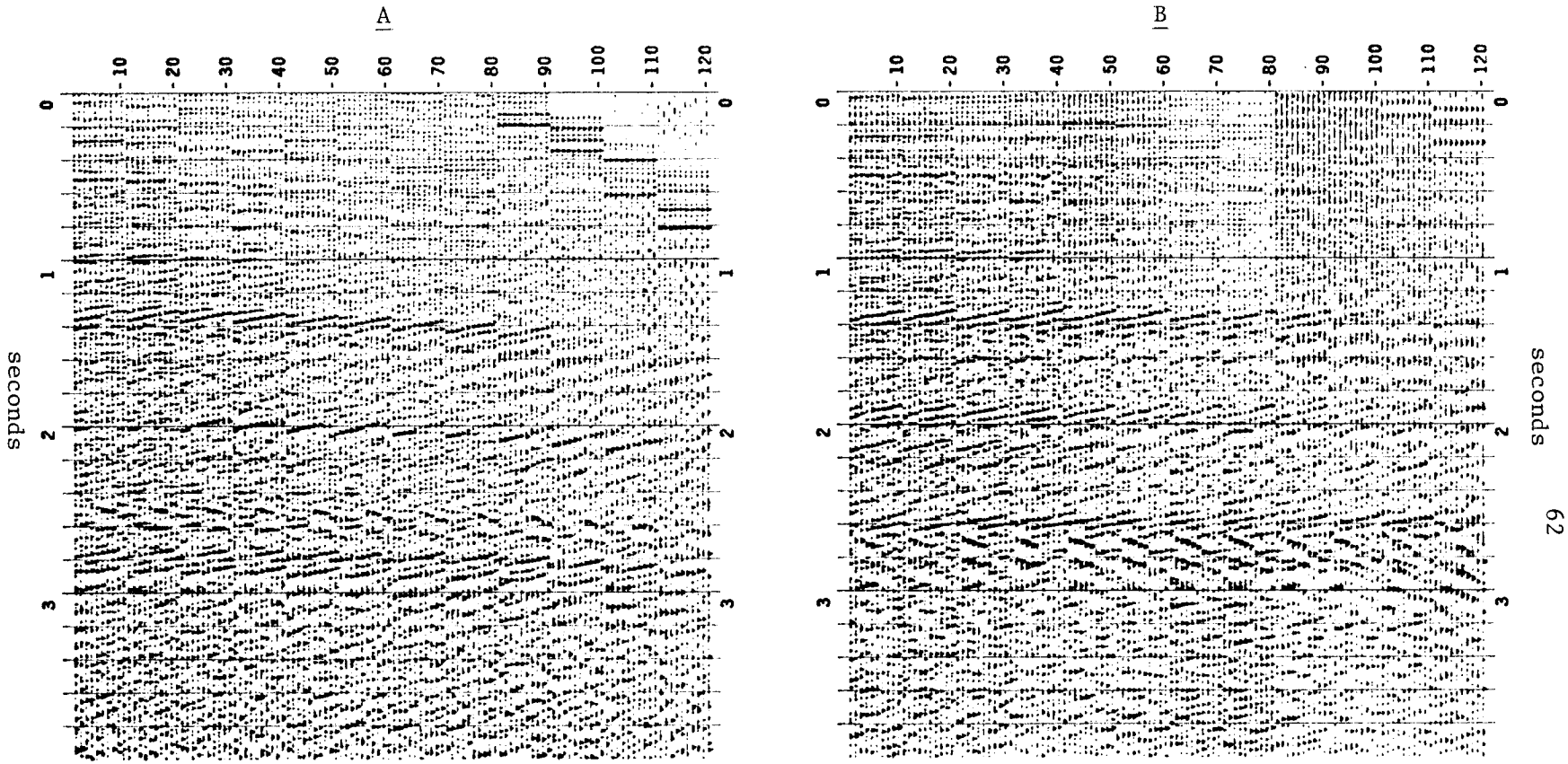

Figure 15. Common midpoint gathers from unmigrated (A) and migrated (B) offsets. Inner twelve offsets displayed. Ten adjacent midpoints between 110 and 120 in figure 14 are shown at each offset. This figure demonstrates that this algorithm automatically performs a normal moveout correction.